NAVAL MEDICAL RESEARCH UNIT SAN ANTONIO

DEVELOPMENT OF MULTIFUNCTIONAL ZnO NANOCARRIERS FOR CONTROLLED AND ENHANCED BIOFILM DISPERSION

ZAKIYA SKEETE, PhD
SARA ROW, MS
DICKSON KIRUI, PhD
NANCY J. MILLENBAUGH, PhD

MAXILLOFACIAL INJURY AND DISEASE DEPARTMENT
CRANIOFACIAL HEALTH AND RESTORATIVE MEDICINE DIRECTORATE

NAMRU-SA REPORT # 2020-05

DECLARATION OF INTEREST

The views expressed in this technical report are those of the authors and do not necessarily reflect the official policy or position of the Department of the Navy, Department of Defense, nor the U.S. Government. This work was funded by the Office of Naval Research's Navy Medicine In-house Laboratory Independent Research Program using work unit number G1701. Some of the authors are employees of the U.S. Government. This work was prepared as part of their official duties. Title 17 USC §105 provides that 'copyright protection under this title is not available for any work of the U.S. Government.' Title 17 USC §101 defines a U.S. Government work as a work prepared by a military service member or employee of the U.S. Government as part of that person's official duties.

ACKNOWLEDGEMENTS

The authors would like to thank Dr. Andrew Zane of the Naval Medical Research Unit San Antonio (NAMRU-SA) for assistance with drafting the proposal and pilot experimentation, Dr. Wen Chen (NAMRU-SA) for assistance with pilot experimentation, and Ms. Iram Qureshi (NAMRU-SA) for help with statistical analysis.

REVIEWED AND APPROVED BY:

10/22/19

Sylvain Cardin, PhD
Chair, Scientific Review Board
Chief Science Director
Naval Medical Research Unit San Antonio
3650 Chambers Pass, BLDG 3610
Fort Sam Houston, TX 78234-6315

Date

2019-10-22

CAPT Andrew F. Vaughn, MC, USN
Commanding Officer
Naval Medical Research Unit San Antonio
3650 Chambers Pass, BLDG 3610
Fort Sam Houston, TX 78234-6315

Date

TABLE OF CONTENTS

I. ABBREVIATIONS

A	Amperes
Å	Angstroms
Ag	Silver
Au	Gold
a.u.	Arbitrary units
BCA	Bicinchoninic acid
Dept. HHS	Department of Health and Human Services
DI water	Deionized water
DLS	Dynamic light scattering
DMSO	Dimethyl sulfoxide
EDTA	Ethylenediaminetetraacetic acid
FDA	Food and Drug Administration
FTIR/FT-NIR	Fourier transform infrared/Fourier transform-near infrared spectroscopy
HCl	Hydrochloric acid
HMT	Hexamethylenetetramine
keV	Kilo-electron-volt
kV	Kilovolt
MΩ	Megaohms
MCA	*N*α-Benzoyl-*L*-arginine-7-amido-4-methylcoumarin hydrochloride
NaOH	Sodium hydroxide
NP(s)	Nanoparticle(s)
PDI	Polydispersity index
P. aeruginosa	*Pseudomonas aeruginosa*
RFU	Relative fluorescent units
rpm	Revolutions per minute
S. aureus	*Staphylococcus aureus*
SEM	Scanning electron microscopy
W	Watts
XRD	X-ray diffraction

ZnO	Zinc oxide
ZnO-Pap	Papain-loaded zinc oxide
λ	Wavelength

1. EXECUTIVE SUMMARY

Background: Treatment failures in chronic, combat-related maxillofacial and oral infections are associated with multidrug-resistant biofilms that hinder the diffusion of antibiotics and block host immune cell function via production of a dense extracellular matrix. A promising strategy for treating biofilm-related infections is the use of enzymatic debridement agents to breakdown the biofilm matrix. Widespread employment of these agents, however, is limited by the lack of appropriate formulations to achieve controlled and sustained delivery.

Objective: Herein, the successful development of zinc oxide (ZnO) nanocarriers containing the natural proteolytic debridement and biofilm dispersal agent papain is reported. ZnO nanomaterials were selected as a delivery system for this study based on their biocompatibility and pH-triggered degradation, which may provide localized drug release at acidic microenvironments typically present within biofilms.

Methods: Papain-loaded ZnO nanoparticles (ZnO-Pap NPs) were synthesized using a protocol adapted from a published sonochemical method. Size and morphology of the ZnO-Pap NPs were characterized by dynamic light scattering (DLS) and scanning electron microscopy (SEM). Incorporation of papain into the ZnO NPs was assessed via Fourier transform infrared spectroscopy (FTIR) and assays for total protein content and protease activity. Stability of the ZnO-Pap NPs was studied over 28 days using DLS and SEM. Dissolution of the ZnO-Pap NPs at pH 5 and 6 was assessed over 24 h via spectrophotometry to confirm acid-induced degradation.

Results: Syntheses resulted in spherical ZnO-Pap NPs with dry diameters of 177 ± 50.2 nm. Loading of papain into the NPs was confirmed by the presence of protein functional groups detected via FTIR. Total papain content was 168 ± 7.85 μg/mg of NPs, and 41% of the protease activity of the loaded papain was retained. After 7 days of storage at room temperature, the particle size varied by >3 standard deviations beyond the mean particle size at day 2, indicating instability of NPs in solution. However, SEM analyses indicated the NPs were structurally stable for 28 days. During the first 1 h of dissolution testing, absorbance of the ZnO-Pap NPs decreased by 74% at pH 5, 27% at pH 6, and 10% at pH 7, confirming acid-induced NP degradation.

Conclusions: Results show reproducible syntheses of ZnO-Pap NPs that were structurally stable for 28 days and exhibited pH-triggered dissolution. Future work will focus on optimization of NP storage conditions to improve dispersion stability, evaluation of strategies to increase papain loading efficiency, and demonstration of ZnO-Pap NP efficacy against bacterial biofilms.

2. INTRODUCTION

Biofilms have a tremendous impact on human health due to their pervasive and recalcitrant nature, which makes them extremely difficult and costly to remove from dental and medical devices, contaminated surfaces in treatment facilities, and infected tissues [1, 2]. The ability of biofilms to successfully survive in a vast range of environments is due to formation of a dense extracellular matrix that serves as a barrier against mechanical and shear stress, chemical disinfectants, host immune system attack, and antibiotics [2]. The dense matrix also creates a milieu that induces drug tolerance in biofilm-associated bacteria, leading to a continued source of microbe dissemination that causes recurrent infections [2]. Indeed, the most severe biofilm infections may persist indefinitely if the infected regions are not effectively removed [3]. Due to this notable persistence, biofilms play a critical role in the pathogenesis of chronic oral and maxillofacial infections such as dental plaque, gingivitis, oral candidiasis, and skin and soft tissue wound infections [4]. Chronic biofilm infections, therefore, have the potential to adversely affect military readiness by complicating the recovery of combat-injured US military personnel and significantly delaying return to duty [5].

Dispersion (detachment) of biofilms via use of enzymatic debridement agents is an attractive approach for treatment of chronic infections because it is potentially effective against a broad range of pathogens, may be less painful and more effective than mechanical dispersion, and can be applied in outpatient dental and medical settings [6]. Enzymatic dispersal agents include proteases, glycosidases, and deoxyribonucleases, all of which remove biofilms by degrading the proteins, polysaccharides, and DNA that form the adhesive components of the matrix. These agents have been used as an essential part of wound care because they remove necrotic tissue, enhance penetration of therapeutic agents, and promote healing [7, 8]. Examples of conventional enzymatic agents include papain/urea, collagenase, and DNase I/fibrolysin [4, 9]. Papain is a protein-digesting, water soluble enzyme obtained from papaya fruit latex that has been proven effective in debridement, as an anti-inflammatory, and for decreasing bioburden in topical wound healing applications [10] and against *in vitro* bacterial biofilms [10, 11]. Our group recently demonstrated that papain dispersed *in vitro* methicillin-resistant *Staphylococcus aureus* biofilms at concentrations of 10 and 25 μg/mL, decreasing biomass by 94-98% after 24 h of treatment [11]. Despite its proven capabilities, the US Food and Drug Administration (FDA) has limited the use of papain due to adverse effects observed in unapproved topical products and limited dosage

studies on the human body [12]. To overcome these concerns, it is imperative to develop novel delivery formulations that can deliver papain to target locations and reduce its negative effects on healthy host tissue while optimizing activity against pathogenic biofilms.

Drug delivery systems based on nanotechnology provide a promising strategy to control the release of therapeutic agents and circumvent negative side effects to a patient's healthy tissue. For example, zinc oxide nanoparticles (ZnO NPs) have been engineered to facilitate localized delivery of chemotherapeutics based on pH-triggered degradation in acidic microenvironments within cells, resulting in controlled dissolution and drug release [13, 14]. This approach may provide enhanced delivery of therapeutic agents, like papain, to acidic microenvironments within biofilms, such as dental plaque.

In addition to acting as carriers, metal oxide NPs such as ZnO NPs [15] exhibit intrinsic antimicrobial activity against planktonic bacteria [16]. ZnO NPs have shown significant antibacterial properties against several multidrug-resistant bacteria including *Pseudomonas aeruginosa, Rothia dentocariosa,* and *Escherichia coli* [17-19]. Resultantly, these NPs have been incorporated into wound dressing fibers and used to prevent *S. aureus* infection and enhance wound healing *in vivo* [20-22]. ZnO NPs are particularly attractive for treatment against bacteria because they are inexpensive, easy to synthesize, and are described as "generally recognized as safe" by the US FDA (21CFR182.8991) [23]. However, while ZnO NPs have shown potency against a variety of planktonic gram-negative, gram-positive, and spore-forming bacteria, they have limited effect against biofilm infections [24-26]. For example, McGuffie *et al.* [25] demonstrated that colloidal suspensions of ZnO NPs caused a 95% reduction in *S. aureus* cell viability, but scanning electron microscopy (SEM) imaging revealed remnant bacterial biofilms existed after treatment.

To effectively address the challenges posed by biofilms, new approaches that leverage the advantages presented by enzymatic dispersal agents and the attractive properties of ZnO NPs are needed. In this study, papain-loaded ZnO NPs (ZnO-Pap) were synthesized following a procedure adapted from Deng *et al.* [27], who reported the formation of hollow ZnO nanoshells by a facile, template-free sonochemical process. This NP synthesis method was selected because of its feasibility for synthesizing large quantities of particles at low temperatures, making it more advantageous for encapsulating thermosensitive materials than other procedures that employ elevated temperatures. Synthesized papain-loaded and unloaded ZnO NPs were characterized by

dynamic light scattering (DLS), x-ray diffraction (XRD), scanning electron microscopy (SEM), ultraviolet-visible (UV-Vis) spectroscopy, and Fourier-transform infrared spectroscopy (FTIR) to determine the optical and physical properties, amount and enzymatic activity of loaded papain, stability under storage, and pH-dependent dissolution. These findings will aid in the development of drug delivery systems for effective treatment and dispersion of biofilm-associated infections.

3. MATERIALS AND METHODS

3.1 Reagents and materials

Hexamethylenetetramine (HMT, ACS grade, ≥ 99.0%), zinc nitrate hexahydrate (reagent grade, 98%), papain from *Carica papaya* (≥ 3 U/mg), *N*α-benzoyl-*L*-arginine-7-amido-4-methylcoumarin hydrochloride (MCA, ≥ 99.0%), sodium phosphate dibasic (BioReagent grade, ≥ 99.0% purity), ethylenediaminetetraacetic acid (EDTA, anhydrous, BioReagent grade), sodium hydroxide (NaOH, reagent grade, ≥ 98%), *L*-cysteine hydrochloride monohydrate (non-animal sources, USP and EP testing specifications), and dimethyl sulfoxide (DMSO, molecular biology grade) were purchased from Sigma Aldrich (St. Louis, MO). Nalgene high-speed 50-mL centrifuge tubes and the Pierce BCA protein assay kit (Catalog No. 23225) were purchased from ThermoFisher Scientific (Waltham, MA). Hydrochloric acid (HCl, TraceMetal™ grade, 34 – 37%) was purchased from Fisher Scientific (Hampton, NH). Deionized (DI) water (18.2 MΩ•cm^{-1}) was obtained from a Millipore water purification system with a BioPak Ultrafilter.

3.2 Nanoparticle synthesis and dehydration

ZnO-Pap NPs were synthesized following a procedure adapted from Deng *et al.* [27]. In brief, 4.20 g of HMT were dissolved in 100 mL of DI water by vigorous stirring, and 50.0 mg of papain were subsequently added. The mixture was continuously stirred for 5 min to ensure complete dissolution. In a secondary beaker, 0.595 g of zinc nitrate hexahydrate was dissolved in 20 mL of DI water under stirring. The zinc nitrate solution was gently added into the HMT-papain solution and mixed for 3 min by vigorous stirring to ensure uniformity. This precursor mixture was sonicated for 20 min at 50 W of output power using a probe sonicator (Qsonica 700 series, Newtown, CT). ZnO NPs (no papain) were prepared in a similar fashion without the addition of papain into the reaction. After sonication, the resulting milky white precipitate was collected in four 50-mL tubes and centrifuged at 5,000 rpm for 30 min (Beckman Coulter Avanti JXN-30, JA-

12 rotor, Pasadena, CA) to recover the resultant NPs. Pelleted NPs were re-suspended in a minimum volume of DI water using a sonicator probe bath, pooled into a single Nalgene centrifuge tube, and centrifuged at 10,000 rpm for 5 min. The NPs were rinsed thrice by repeated re-suspension of the pellet in DI water and centrifugation at 10,000 rpm for 5 min to ensure complete removal of precursor materials. After the final rinse, NPs were re-suspended in 20 mL of DI water using the sonicator probe bath. NPs were either stored in water ("as-synthesized") at room temperature or dried. To dry the NPs, the suspension was aliquoted into 1.5-mL Eppendorf tubes and dehydrated in a Savant SpeedVac (ThermoFisher Scientific) at a vacuum rate of 40 torr/min for 210 min with heating at 45°C for the first 150 min of the cycle. Dehydrated NPs were stored in a desiccator at room temperature until use.

3.3 Size and surface charge characterization

Nanoparticle size and surface charge distribution were characterized using a Malvern Zetasizer Nano-ZS (Westborough, MA). NPs were diluted 100-fold in DI water, particle size was measured via DLS, and the surface charge (zeta potential) was measured via electrophoretic light scattering techniques following protocols described in the Malvern user manual. Samples diluted in DI water were added into clear disposable zeta cells and equilibrated to 25°C for 180 s prior to acquiring size or zeta potential readings.

3.4 SEM analysis

SEM imaging was used for visualization of ZnO and ZnO-Pap NPs to confirm size and morphology. Samples were prepared by drop-casting 20 µL of NP suspension on a glass substrate and dehydrating samples under vacuum overnight. After mounting the glass onto a specimen stub using carbon tape, samples were sputter-coated with a gold-palladium (50%-50%) target using a Leica EM ACE600 sputter coater (Buffalo Grove, IL) and imaged using a Sigma-VP40 field emission scanning electron microscope (Carl Zeiss Inc., Jena, Germany) under high vacuum. Images were acquired at a working distance of 5-8 mm with an energy differential of 2 kV and magnifications up to 20,000×. SEM micrographs were used to visualize size and NP morphology over time in samples stored dried or as a suspension in water. Dimensions of particles were measured in pixels and converted to nanometers using the scale bars.

3.5 FTIR analysis

Surface characterization via FTIR was used to determine papain incorporation into ZnO NPs. Dehydrated NPs were placed on the universal attenuated total reflection accessory and scanned from 650 to 4000 cm^{-1} at a resolution of 2 cm^{-1} using a Perkin Elmer Spectrum 400 spectrometer (Waltham, MA). To obtain a good signal/noise ratio, 32 scans were collected and averaged. Incorporation of papain was assessed based on comparison of FTIR absorption peaks present in ZnO-Pap NPs and ZnO NPs.

3.6 XRD analysis

XRD patterns of ZnO and ZnO-Pap NPs were obtained using a Bruker D8 Discover x-ray diffractometer (Billerica, MA). NP suspensions were prepared by 100-fold dilutions in DI water, drop-casted on a silica zero diffraction plate, and dried in a vacuum desiccator. XRD patterns were performed by Cu-Kα radiation with a λ of 1.54 Å, voltage of 40 keV, and tube current of 40 mA. The scanning was conducted between 10.0° to 87.6° of 2θ with a step-size of 0.02° and 90 s per step.

3.7 Total protein quantification assay

The amount of papain in the NPs was determined using a Pierce BCA assay kit according to the manufacturer's protocol. Dehydrated ZnO-Pap and ZnO NPs (day 2 - day after synthesis) were re-suspended at 2 mg/mL using 0.1 M HCl and allowed to digest for 24 h at 4°C. A stock solution of papain (2 mg/mL) was freshly prepared in 0.1 M HCl and serially diluted into 9 standards (0, 25, 125, 250, 500, 750, 1000, 1500, and 2000 µg/mL). The working reagent was prepared by mixing reagent A with reagent B from the kit at a 50:1 ratio. Samples were prepared by adding 25 µL of sample and 200 µL of the working reagent into a 96-well plate. The samples were briefly mixed by shaking in a Tecan Spark 10M multimodal microplate reader (Durham, NC) and incubated at 37°C for 30 min in the dark. Absorbance was measured at 562 nm, and the amount of papain in each unknown sample was calculated in GraphPad Prism 6 software (Version 6.07, San Diego, CA) using a standard curve.

3.8 Enzymatic activity assay

Enzymatic activity of ZnO-Pap NPs was assessed following a procedure adapted from Pinto *et al.* [28] using MCA as the substrate. A stock solution of 10 mM MCA was prepared in DMSO, stored at -20^{o}C, and thawed immediately before use. The buffer (250 mL) was prepared by dissolving 365 mg of EDTA, 219 mg of *L*-cysteine hydrochloride monohydrate, and 3.54 g of sodium phosphate dibasic in DI water under vigorous stirring and heating. MCA/buffer solution was prepared by mixing 7 µL of MCA with 25 µL of cold (4°C) buffer for each sample well. All the reagents were kept at 4°C or under ice during sample preparation, and the Tecan microplate reader was pre-heated to 40°C. Papain standards (0.1, 0.2, 0.5, 1, 2, 5, and 10 µg/mL equivalent to 3×10^{-4}, 6×10^{-4}, 1.5×10^{-3}, 3×10^{-3}, 6×10^{-3}, 0.015, and 0.03 U/mL) were prepared from a papain stock solution (2 mg/mL or 15 U/mL in water), and dehydrated (day 2) NP samples were re-suspended in DI water at 0.02, 0.2, and 2 mg/mL to ensure fluorescent readings would fall within the calibration curve range. Into each well of a 96-well plate, 55 µL of buffer solution, 30 µL of standard or NP suspension, and 30 µL of the pre-chilled, freshly diluted MCA/buffer solution were sequentially added. Before measurement, sample plates were mixed by brief agitation. Fluorescent intensity readings in relative fluorescent units (RFU) were acquired using 360/460 nm excitation/emission wavelengths at 5 min intervals for 60 min. The scans were acquired with 30 flashes at a 40 µs integration time and optimal gain setting. The RFU data over time (min) was used to calculate a slope (RFU/min) for each standard and NP sample using the linear regression function in GraphPad Prism 6 software. The slopes in RFU/min for the standards were plotted against known activity (U/mL) to generate a standard curve, which was then used to calculate activity (U/mL) in the NP samples.

3.9 pH titration and NP dissolution

Dissolution of the NPs in acidic conditions was first evaluated over a wide pH range using a Malvern Zetasizer Nano-ZS with multipurpose titrator (MPT-2). Dehydrated (day 2) NPs were re-suspended at 2 mg/mL in DI water via water bath sonication (2 min) and diluted to 0.2 mg/mL in 5-mL working volumes. The pH probe was calibrated before each experiment using standards at pH 4, 7, and 10. Titrations were performed starting from the native, unadjusted pH (pH ~ 7.4), which was decreased in increments of 0.3 pH units (pH tolerance = 0.1) with auto-titrator injections of 0.1 M HCl until pH 3 was attained. Particle size and zeta potential were determined at each

increment. An aqueous papain solution (416.7 mg/mL) was spiked with 20 µL of 0.1 M NaOH to increase the pH to ~ 8 and titrated as a control for comparison.

Subsequent dissolution experiments were conducted by re-suspending dehydrated (day 2) NPs in DI water using a sonicator probe to 0.2 mg/mL. The pH of the NP samples was adjusted to 5 or 6 by dropwise additions of 1 M HCl or left unadjusted (~ pH 7.4; "neutral") for use as controls. At various time points over a 24-h period (t = 0, 1, 2, 3, 5 and 24 h), the samples were sonicated for 2 min and 200-µL aliquots were removed for measurement of NP absorbance at 370 nm using a BioTek Synergy H1 Hybrid Reader (Winooski, VT). Prior to data acquisition, samples were briefly agitated (5 s, 365 rpm) in the plate reader to minimize NP settling.

3.10 Statistical analysis

Data are presented as the average ± standard deviation unless otherwise stated. NP dissolution data in Figure 7 were analyzed using GraphPad Prism software, in which one-way analysis of variance and post hoc Tukey multiple comparison tests were employed to compare differences between treatment groups. A value of $p < 0.05$ was considered statistically significant.

4. RESULTS AND DISCUSSION

4.1 NP physical and chemical property analysis

Multiple batches of ZnO and ZnO-Pap NPs were synthesized sonochemically and characterized via DLS and SEM the day after synthesis (day 2) to determine particle size distribution and morphology. **Figure 1A** portrays a representative DLS histogram of a single batch of ZnO NPs with an average hydrodynamic particle size (Z-average) of 483 ± 34.3 nm, a peak size of 499 ± 47.6 nm, and a polydispersity index (PDI) of 0.224. The histogram showed the ZnO NPs had a narrow size distribution with one prominent main peak and a secondary peak between 4 and 6 µm that represents only 2% of the total peak area. The similarity of the Z-average and peak size values and the low PDI value also indicated that the sample was monodispersed. **Figure 1B** shows representative DLS data for a single ZnO-Pap NP batch with a Z-average of 524 ± 52.8 nm, peak size of 395 ± 60.0 nm, and PDI of 0.530. Though the histogram for the ZnO-Pap NPs shows only one prominent peak and one minor peak, the high PDI value and disparity between the Z-average and peak size values indicated that the size of these NPs were more broadly distributed than the ZnO NPs and may have contained large aggregates (> 10,000 nm). Over 14 individual batches of

ZnO NPs, the average hydrodynamic particle size was 429 ± 86.8 nm with an average PDI of 0.264 ± 0.136. Conversely, 12 batches of ZnO-Pap particles had a mean Z-average of 563 ± 147 nm with an average PDI of 0.517 ± 0.0756. Based on these analyses, it was evident that the inclusion of papain into ZnO NPs widened the size distribution of the samples. These results suggest that papain decreased the dispersion stability of the NPs or caused formation of aggregates during the synthesis process.

To confirm the size and morphology of the NPs, SEM was used to analyze select samples. The SEM images revealed that ZnO NPs were prolate spheroid, hollow shell structures comprised of elongated ZnO platelets (**Figure 1C**). Analysis of the size of one batch of dehydrated NPs showed an average width of 145 ± 32.7 nm (N = 91) and length of 317 ± 41.9 nm (N = 23). The difference in NP sizes obtained from DLS and SEM is likely due to the outer hydration layer surrounding NPs in solution that is measured via DLS but is absent in the dehydrated NPs analyzed by SEM. The ZnO NPs were similar in size to those reported by Deng *et al.* [27], which were approximately 500-nm hollow shells with a 400-nm interior. However, the particles synthesized by Deng *et al.* were spherical unlike the elongated particles obtained in the current study (**Figure 1C**). This could be due to differences in NP synthesis methodology between the two studies, such as reaction volumes and the type of sonicator employed, that caused differences in reaction temperatures and rates. The ZnO NPs from the current study were also similar in size to ZnO nanoshells synthesized by Zhao and Qi [29] using a microwave assisted solvothermal method that ranged from 400 to 700 nm in diameter.

In contrast to results from the ZnO NPs, the SEM micrographs of ZnO-Pap NPs revealed that the addition of papain into the reaction resulted in the formation of spherical NPs (**Figure 1D**). The change in NP morphology caused by addition of papain could be due to the interactions between the papain and ZnO surfaces as the particle forms. This is supported by the presence of smoother surfaces on the ZnO-Pap NPs compared to the ZnO NPs when observed at higher image magnifications (50,000×). The SEM micrographs from a single batch of ZnO-Pap NPs revealed an average particle size of 177 ± 50.2 nm (N = 74), which was consistent with the widthwise dimensions of the ZnO NPs. The higher magnification (50,000×) images also showed that both ZnO and ZnO-Pap NPs were comprised of two fused hemispheres with a hollow interior, which was apparent in SEM images of fragmented NPs (**Figures 1C and 1D** insets). From these images,

it was evident that the incorporation of papain did not adversely affect the formation or structural integrity of the ZnO-Pap NPs.

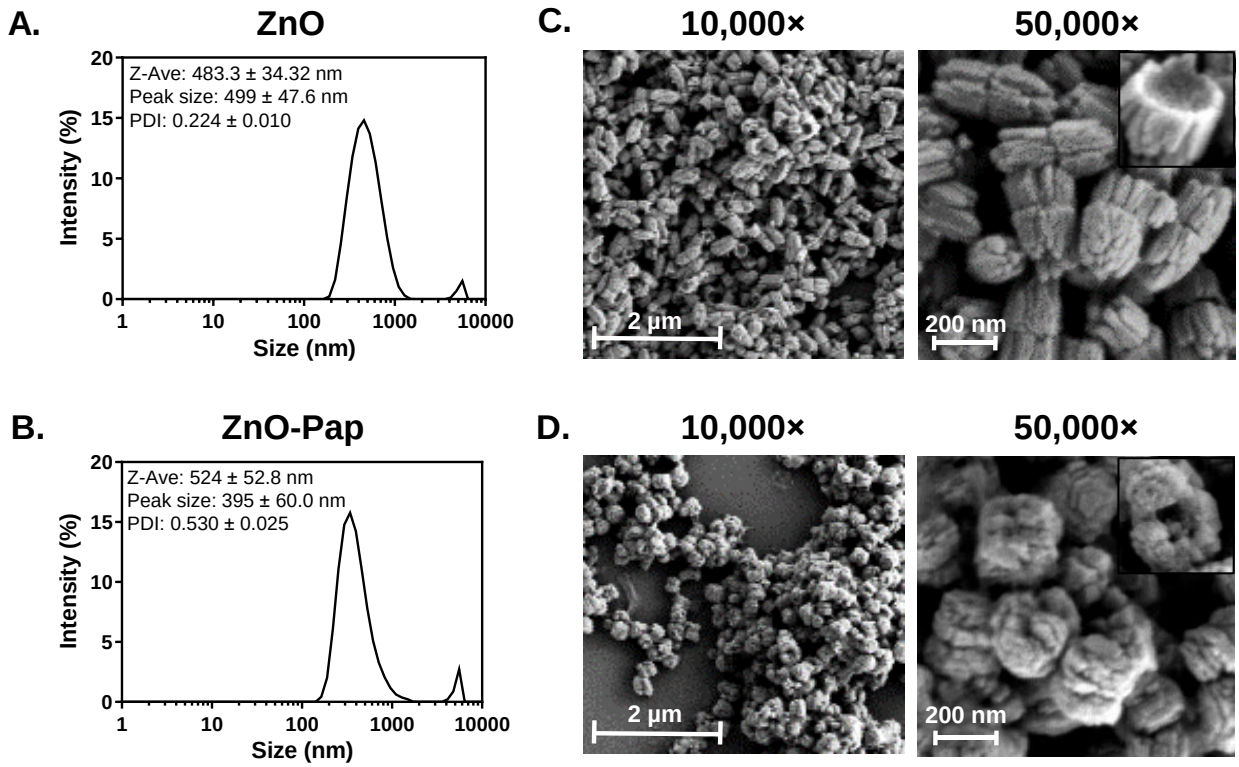

Figure 1. DLS and SEM characterization of ZnO and ZnO-Pap NPs. DLS size distribution analyses of A) ZnO and B) ZnO-Pap NPs. C) ZnO NP micrographs captured at 10,000× (top left) and 50,000× (top right) magnification. D) ZnO-Pap NP micrographs captured at 10,000× (bottom left) and 50,000× (bottom right) magnification. Images of fragmented NPs (insets) acquired at 50,000× magnification revealed hollow hemispherical NPs.

The structures of papain-loaded and unloaded NPs were subsequently analyzed by XRD. Representative XRD patterns of the ZnO and ZnO-Pap NPs are shown in **Figures 2A**. The diffraction patterns of the ZnO phase was observed at $2\Theta = 30$, 35, and 55.5^{o} for ZnO and ZnO-Pap NPs (**Figure 2A**). These patterns are characteristic of ZnO's hexagonal wurtzite crystalline structure as reported in the Joint Committee on Powder Diffraction Standards card 5-664 and peer-reviewed literature [15, 27, 29, 30]. XRD analyses of ZnO-Pap NPs did not show any patterns for papain, potentially due to the instrument's limit of detection. Similar findings have been previously reported in the literature, which also showed ZnO NPs did not display any notable peak changes in XRD patterns upon drug loading [31]. It was also notable in the current study that incorporation of papain did not appear to alter the crystal structure of ZnO, which may also be due to the small

amount of papain in the NPs (**Figure 2A**). In addition, XRD patterns of reaction precursors, HMT and zinc nitrate (**Figure 2B**), showed distinct phases which were absent in the resultant NPs (**Figure 2A**). These results indicate effective removal of unreacted precursors from the purified NP samples.

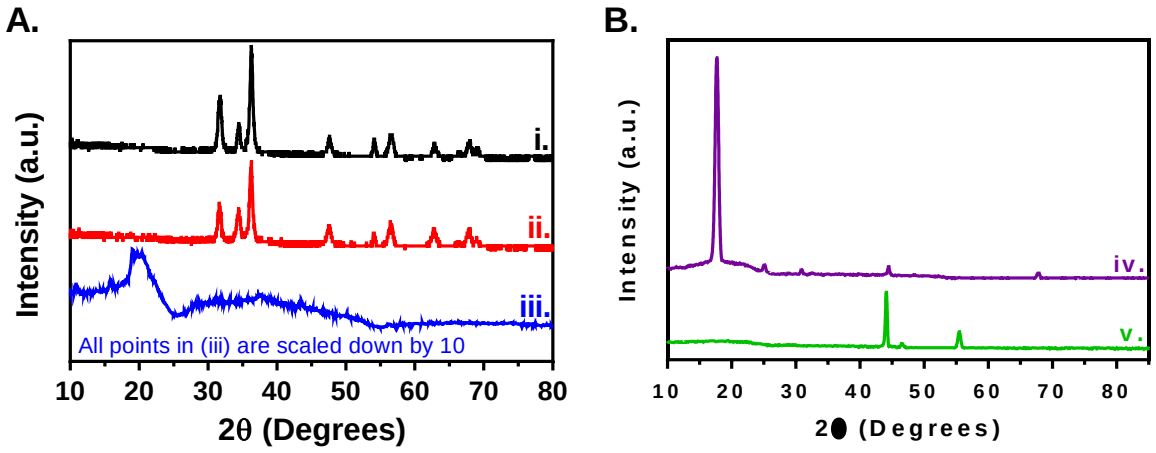

Figure 2. XRD patterns of ZnO and ZnO-Pap NPs. A) XRD patterns of (i) ZnO NPs, (ii) ZnO-Pap NPs, and (iii) papain. B) XRD patterns of the synthetic precursors (iv) HMT and (v) zinc nitrate. Note that a.u. denotes arbitrary units.

The presence of papain in ZnO-Pap NPs was assessed by FTIR spectroscopy (**Figure 3A**). The expected functional groups and respective wavenumbers associated with the presence of proteins are presented in **Table 1**. The ZnO-Pap NP spectrum revealed bond vibrational and stretching modes which are characteristic of amide groups: peaks at 3400 – 3500, 1660, and 1534 cm^{-1} are due to vibrational, symmetric and asymmetric stretching of N-H bonds; a peak at 1026 cm^{-1} for C-N bond stretching; and peaks at 1670 and 1820 cm^{-1} for C=O bond stretching. The spectrum further revealed a peak shift at ~ 900 cm^{-1} indicating the transformation of a metal hydroxide to a metal bound carbon or nitrogen. Notably, the distinct peaks observed in the ZnO-Pap NP spectrum were present in the papain only scan but absent in the ZnO NP spectrum, which confirmed successful incorporation of papain (**Figure 3A**). Additionally, these FTIR patterns were consistent with those reported in the literature for papain, ZnO, and drug-loaded ZnO NPs [30-32]. In agreement with the XRD data, the ZnO NP and ZnO-Pap NP spectra did not exhibit all of the major peaks associated with the presence of HMT or zinc nitrate precursors (**Figure 3B**), confirming that purified NPs did not contain detectable amounts of unreacted precursors.

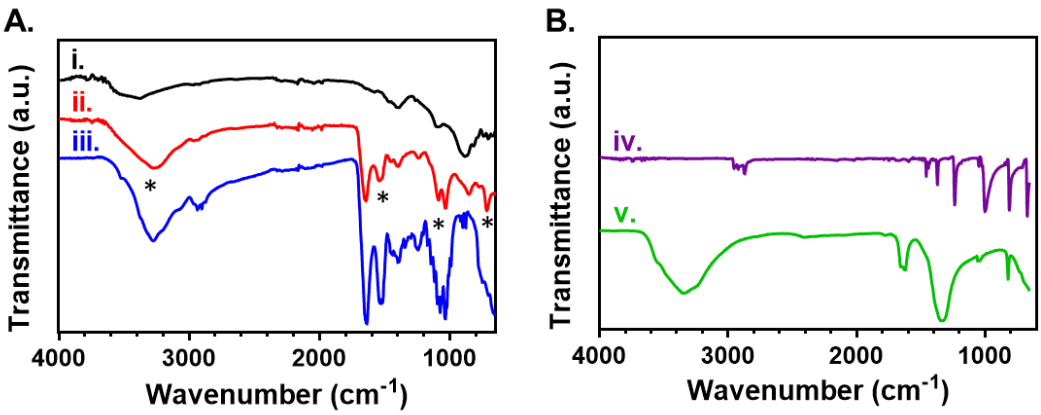

Figure 3. FTIR spectra of ZnO and ZnO-Pap NPs. A) FTIR spectra of (i) ZnO NPs, (ii) ZnO-Pap NPs and (iii) papain. B) FTIR spectra of the synthetic precursors (iv) HMT and (v) zinc nitrate. Asterisks (*) in FTIR scans denote the peak differences between papain-loaded and unloaded ZnO NPs attributed to the presence of papain in ZnO-Pap NP samples. Note that a.u. denotes arbitrary units.

Table 1. Expected Functional Groups Observed in FTIR Spectra for Proteins

Functional Group	Wavenumber (cm^{-1})
Hydroxyl (O-H)	3500-3100
Amine (N-H)	3500-3400, 1600-1500, 1360-1080
Ether (C-O)	1300-1000
Carbonyl (C=O)	1820-1670
Alkane (C-C)	1200-800
Alkane (C-H)	900-650

4.2 Quantification of protein content and enzymatic activity

The amount of papain incorporated into ZnO-Pap NPs from three independent batches was quantified using a colorimetric BCA protein kit to measure total protein and an enzymatic assay with the fluorogenic substrate MCA to measure proteolytic activity. Analysis of total protein revealed that 167.8 ± 7.85 µg of papain was successfully loaded into each mg of ZnO-Pap NPs, corresponding to an 81% loading efficiency (**Table 2**). The MCA enzymatic assay revealed 0.202

± 0.0310 U/mg, which translates to 68.0 µg of active papain per mg of loaded NPs. This concentration corresponds to a 41% recovery of active papain in the system (**Table 2**). These results indicate it may be possible, depending on the rate of release from the NPs, to achieve target papain concentrations of at least 10 – 25 µg/mL (0.03 – 0.075 U/mL) that we previously found were required for effective dispersal of *in vitro* bacterial biofilms [11]. Compared to other papain carrier systems reported in the literature, the sonochemically synthesized NPs in the current study encapsulated approximately twenty-fold less papain (amount of papain/mg of particles) than microparticles (~ 50 – 600 µm) synthesized by double emulsion solvent evaporation [33]. However, increasing particle size can significantly decrease encapsulation efficiency [33], and thus further testing is required to determine the effect of increasing ZnO NP size on papain loading efficiency.

Table 2. Total protein content and enzymatic activity of ZnO-Pap NPs (n=3 batches)

Protein Content from BCA Analysis	Activity from MCA Analysis	Protein Content from MCA Analysis	Percent Active Papain Present
µg/mg NP	U/mg NP	µg/mg NP	%
167.8 ± 7.85	0.202 ± 0.031	68.0 ± 10.4	41%

4.3 Dispersion and structural stability of ZnO and papain-loaded ZnO NPs during storage

Stability of a single batch of ZnO and ZnO-Pap NPs stored suspended in DI water or dehydrated was assessed based on changes in Z-averages over time. The mean Z-average of day 2 dried NPs from multiple independent batches (n = 14 for ZnO NPs and n = 12 for ZnO-Pap NPs) was considered the baseline condition for this set of experiments. Therefore, the average ± 2 standard deviations of the Z-averages for all batches of day 2 dried ZnO or ZnO-Pap NPs was calculated and used as a criterion to assess storage stability (see dotted and dashed lines in **Figure 4A, B**). ZnO NPs showed minimal size changes and the average size of the NPs remained within 2 standard deviations of the baseline Z-average throughout the 28 days of storage in both dried and suspended samples (**Figure 4A**). In contrast, Z-averages of ZnO-Pap NPs increased by day 2 and varied by more than 2 standard deviations by day 3 and 4 for particles stored dried or in water,

respectively (**Figure 4B**). These findings suggest ZnO-Pap NPs stored dried or in water were prone to significant aggregation starting at day 2 after synthesis.

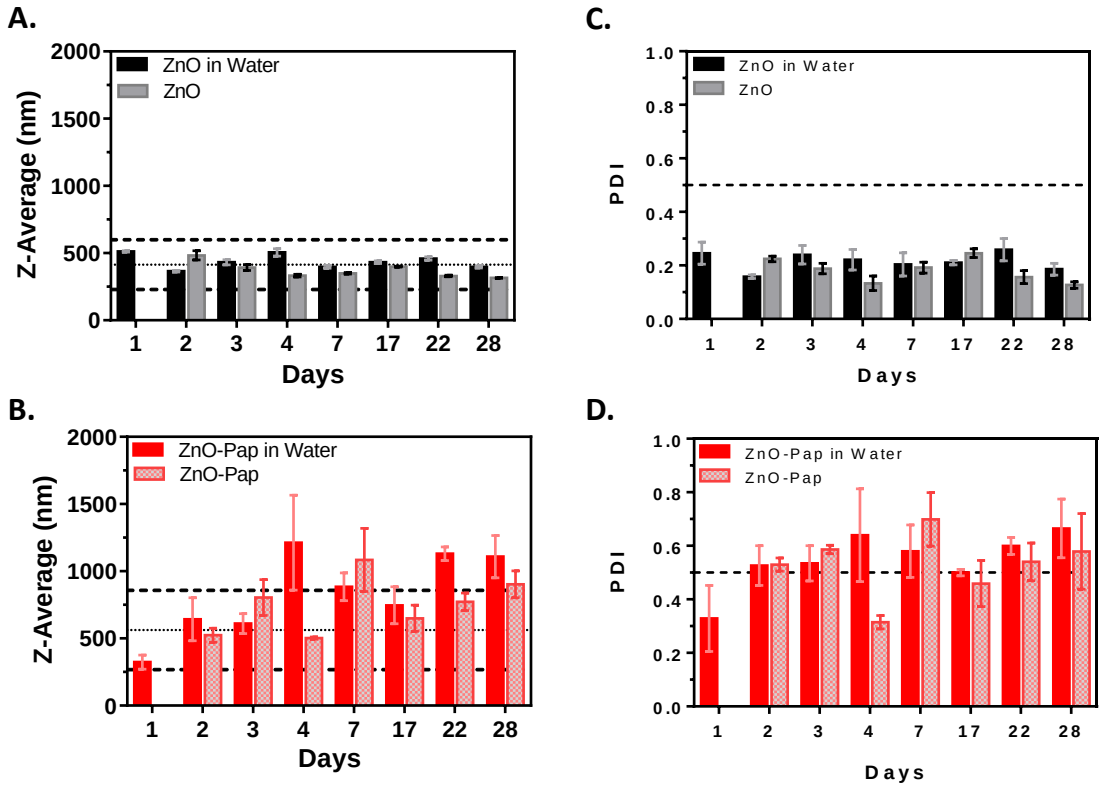

Figure 4. Size distribution and stability of ZnO and ZnO-Pap NPs during 28 days of storage. DLS analysis was used to assess the average size and corresponding polydispersity index (PDI) of (A, B) ZnO NPs and (C, D) ZnO-Pap NPs stored as a suspension in water or dehydrated. Bars and error bars represent the average ± standard deviation from a single batch of ZnO or ZnO-Pap NPs. Dotted and dashed lines in Z-average graphs (A, B) indicate the mean ± 2 standard deviations of Z-averages for day 2 dried particles from all 14 batches of ZnO NPs or 12 batches of ZnO-Pap NPs. Dashed lines in PDI graphs (C, D) indicate the boundary of particle instability at PDI = 0.5.

The PDI of the NPs was also determined to further assess the amount of variance in NP size during storage. ZnO NPs exhibited PDI values < 0.5 when stored dried or in water, which indicated a narrow NP size distribution throughout the entire 28-day storage period (**Figure 4C**). In contrast, ZnO-Pap NPs showed PDI values that increased to > 0.5 and stabilized at day 2 (**Figure 4D**), which coincided with the presence of bi- or multimodal distributions on the size histograms (data not shown). Therefore, the incorporation of papain into ZnO NPs resulted in particles that were less stable and exhibited multimodal size ranges during storage. Based on these findings, optimal conditions need to be determined to increase stability of the ZnO-Pap NPs against aggregation

during storage. Overall, no consistent differences in Z-averages and PDI values were observed during storage between dried NPs and NPs stored in water. However, due to papain's susceptibility to hydrolysis, dry storage conditions may be more suitable.

SEM micrographs were obtained to assess changes in structural morphology over 28 days of storage. Morphology of the ZnO NPs (**Figure 5**, top panel) and papain-loaded ZnO NPs (**Figure 5**, bottom panel) showed no discernable changes over 28 days, suggesting that the NPs have a robust structure. Although the DLS demonstrates that these particles are prone to aggregation, they appear to be stable, individual entities.

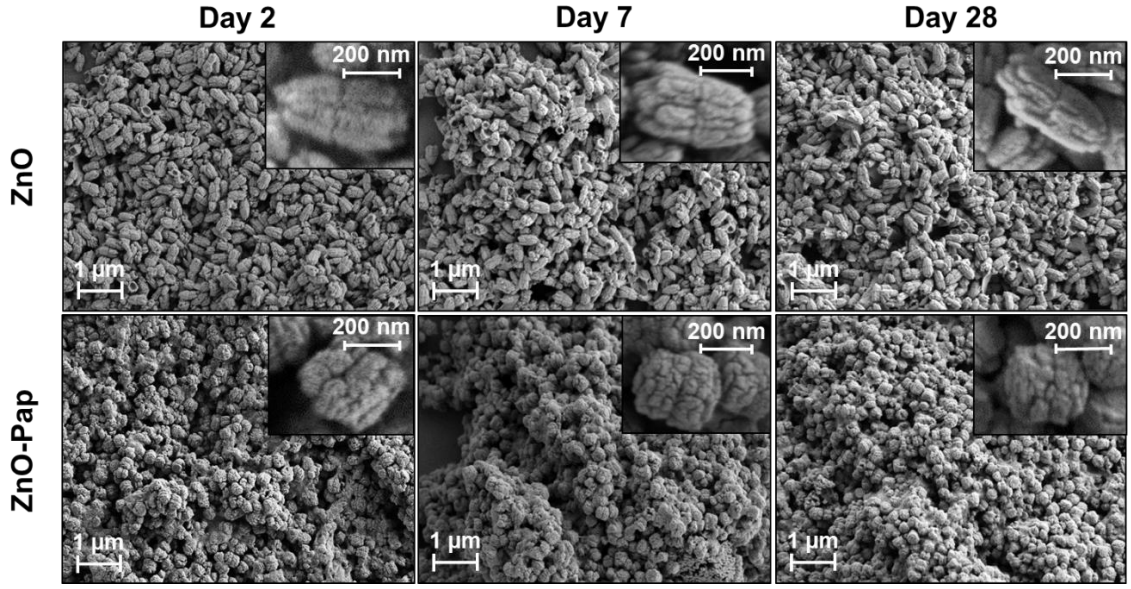

Figure 5. SEM micrographs of dehydrated ZnO and ZnO-Pap NPs showing time-course stability over 28 days. Top panels show micrographs of ZnO NPs and bottom panels show micrographs of ZnO-Pap NPs stored for 28 days. Images showed minimal structural changes in NPs after this duration, suggesting structural stability. Images were obtained at 10,000 × and 50,000 × (image insets).

4.4 pH titration and acid-induced NP dissolution

The effect of pH on Z-average and surface charge of the NPs was assessed through titration assays to determine pH values to use in subsequent studies of acid-induced NP dissolution. Specifically, pH ranges corresponding to transitions in NP stability (zeta potential), sample color, and NP size (Z-average) were of interest because these changes indicate NP dissolution may be occurring. Titration data revealed that the average size of ZnO NPs at pH ≥ 7 was 450 ± 0.448 nm, indicating good particle stability and size uniformity (**Figure 6A**). However, the Z-average

increased to 1165 nm at pH 6.5, suggesting NP aggregation resulting from particle instability at this pH below the zero charge point [34]. Particle size then decreased as the pH decreased below 6.5, and at pH 5, samples exhibited a rapid transition from a cloudy to colorless solution. This indicated possible NP precipitation or dissolution or oxidation of zinc into its ionic form. The zeta potential (surface charge) of ZnO NPs remained relatively constant from pH 7.3 to 5.3, but as pH dropped below 5.3, zeta potential began to increase from -22 mV until it reached a maximum of +22 mV at pH 3.1. Overall, the pH range of 5 to 6.5 was associated with notable transitions in surface charge, size, and sample color for ZnO NPs.

Titration plots of ZnO-Pap NPs (**Figure 6B**) and papain alone (**Figure 6C**) exhibited similar Z-average patterns, i.e., large Z-average values at a neutral pH of 7.3 that decreased rapidly as the pH dropped to 6.1–6.2 and then decreased more slowly or stayed constant at pH < 6.1. This similarity in Z-average patterns indicated the reduction in the hydrodynamic diameter of the ZnO-Pap NPs at acidic pH values may be due, at least in part, to acid-induced changes in the protein structure of papain on the NPs. It was also noted that the surface charge of papain increased by ~ 7 mV from pH 7.4 to 4.6 (**Figure 6C**), suggesting the addition of protons (protonation) to papain induced conformational changes that led to the decreases in hydrodynamic diameters of free papain and the ZnO-Pap NPs. Therefore, optimizing the encapsulation of papain by modifying the electrostatic charges could further stabilize the particles in the presence of water. In contrast to free papain, the surface charge of the ZnO-Pap NPs (**Figure 6B**) showed a similar pattern as that of the ZnO NPs, namely, minor changes in zeta potential from pH 7.3 to 5.3 followed by a more rapid and continual increase as pH decreased from 5.3 to 3.1. Though the changes in the Z-average for the ZnO-Pap NPs during the titration assay did not indicate a definite pH range for NP dissolution, the results showed a transition in zeta potential occurred between pH 5 and 6. The transitions in Z-average, zeta potential, and sample color between pH 5 and 6.5 for ZnO NPs and in zeta potential at pH 5.3 for ZnO-Pap NPs indicated the pH ranges of NP instability. Thus, pH 5 and 6 were chosen for subsequent dissolution experiments.

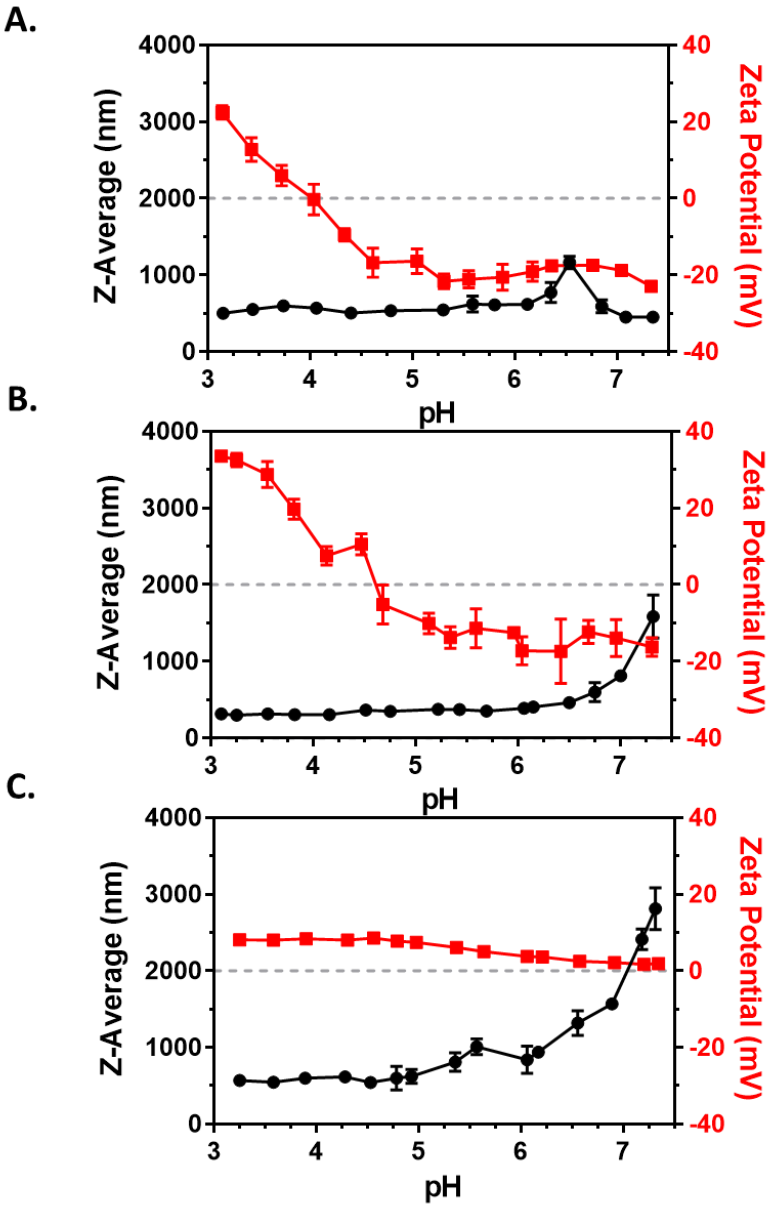

Figure 6. Titration plots showing pH-dependent particle size (black circles) and zeta potential (red squares) of A) ZnO NPs, B) ZnO-Pap NPs, and C) papain only. Titration of NPs was begun at native pH after suspension of NPs in DI water, and papain titration was begun at pH 8 after addition of 0.1 M NaOH. pH was then decreased at intervals of 0.3 pH units by addition of 0.1 M HCl.

Dissolution of ZnO and ZnO-Pap NPs at three different pH values (5, 6, and neutral (control; ~ 7.4)) was evaluated by monitoring absorbance of the NPs at 370 nm for up to 24 h. After 1 h of incubation, the absorbance of ZnO NPs decreased from 1.6 to 0.27 (83% decrease) and 0.41 (74% decline) at pH 5 and 6, respectively (**Figure 7A**), but remained constant at neutral pH, indicating

rapid and significant acid-induced NP breakdown and dissolution. Similar to observations during the pH titration, the ZnO NP samples appeared more translucent as the pH decreased and eventually turned colorless at pH 5. The absorbance of ZnO NPs at neutral pH decreased from 1.6 at 0 h to 1.0 (35% reduction) at 24 h, which could be attributed to stirring of the sample (**Figure 7A**). The absorbance of ZnO-Pap NPs decreased from 0.10 to 0.026 (74% decline) at pH 5, 0.073 (27% decrease) at pH 6, and 0.090 (10% reduction) at neutral pH after 1 h of incubation (**Figure 7B**), suggesting acid-dependent rates of dissolution in these NPs. Additionally, it was observed that ZnO-Pap NPs at pH 5 increased in absorbance from 3 to 24 h of incubation instead of remaining constant or decreasing in absorbance as with ZnO NPs (**Figure 7B**). This phenomenon could be due to the aggregation of free papain in solution after acidification [35]. Thus, the presence of papain appears to affect the manner and the rate of ZnO dissolution in acidic pH conditions, resulting in uneven and slower rates of dissolution compared to ZnO NPs. Overall, these findings are in agreement with reports in the literature of dissolution of drug-loaded ZnO NPs at pH 5 and 6, which show near instantaneous dissolution at pH 5 [31].

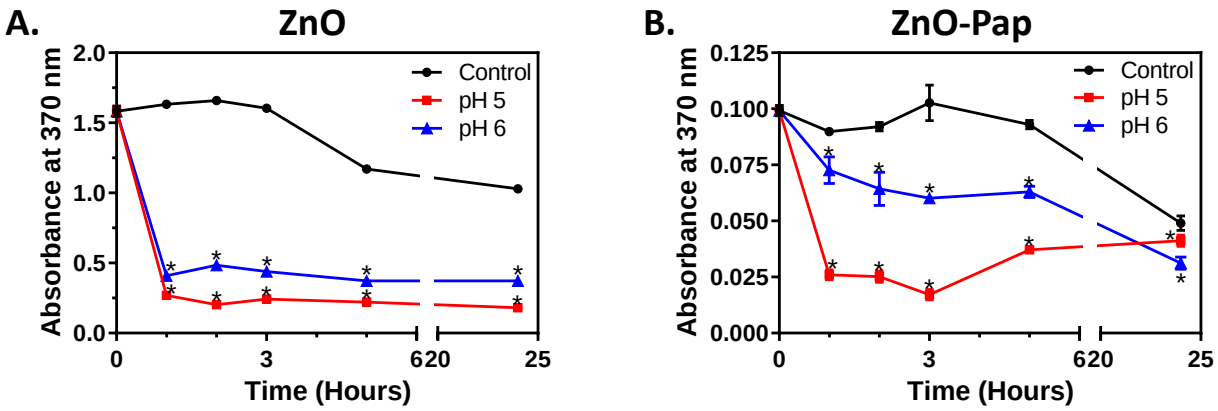

Figure 7. Dissolution kinetics of ZnO and ZnO-Pap NPs in acidic solutions. Time-course changes in absorbance of A) ZnO NPs and B) ZnO-Pap NPs at pH 5 (red squares), pH 6 (blue triangles), or neutral pH (control, black circles). Solutions were incubated with stirring and aliquoted at prescribed time-points for up to 24 h. Absorbance readings were acquired at $\lambda = 370$ nm (n=6). Data are from one representative experiment with six replicate samples per condition. Asterisks (*) indicate $p < 0.05$ compared to the control group at the associated time-point as determined using one-way analysis of variance and post hoc Tukey tests.

5. CONCLUSION AND FUTURE WORK

Successful formation of hollow ZnO NPs was accomplished resulting in particles with a similar size, but slightly different morphology than NPs reported by Deng *et al.* [27]. Papain was successfully introduced into the structure of the ZnO nanoshells, as observed by the presence of carboxylic acid and amine functional groups in the FTIR spectra. The amount of active papain within ZnO-Pap NPs was comparable to that previously used by our group to effectively disperse bacterial biofilms [11]. NP analyses also showed that papain altered the physical appearance but had little influence on the surface chemistry (zeta potential) of ZnO NPs (**Figure 6**). In addition, papain significantly increased aggregation but had no apparent effect on the structural integrity of the NPs during 28 days of storage (**Figure 5**). Further analyses revealed no differences in dispersion stability and structural integrity (Z-average, PDI, and morphology via SEM) over time for dried NPs and particles stored in water; however, dried samples may be more advantageous for promoting papain stability. Both ZnO and ZnO-Pap NP systems demonstrated acid-induced dissolution at pH 5 and 6, but the optimal pH for NP dissolution was determined to be pH 5 based on dissolution rate and transitions in NP color, size, and surface charge. The effect of pH on release of active papain from the NPs, however, remains to be determined. Based on the results of this study, future efforts will focus on optimization of particle stability during storage via use of biocompatible capping agents, such as polyethylene glycol (PEG), to decrease NP aggregation and aid in the stability and release of the papain. Future development will also involve optimization of papain loading efficiency and investigation of papain release kinetics.

6. MILITARY SIGNIFICANCE

Biofilm contamination of wounds is problematic for the successful treatment of US military personnel because it is associated with increased morbidity and mortality rates, higher economic burden, and decreased military readiness. The development and implementation of ZnO nanocarriers for the delivery of dispersal agents would provide a critical tool to enhance treatment of chronic biofilm infections in military personnel. The current report provides a strong framework for the development of a new therapeutic platform that can be incorporated into field deployable wound dressings for the treatment and ultimate prevention of biofilm infections. The ability to encapsulate an active dispersal agent and demonstrate pH-dependent dissolution indicates this

nanocarrier system also shows promise for the delivery of active compounds to target sites in other applications, such as treatment of dental caries or decontamination of abiotic surfaces.

7. REFERENCES

1. Mathur, H., et al., *Fighting biofilms with lantibiotics and other groups of bacteriocins.* NPJ Biofilms and Microbiomes, 2018. **4**(9): p. 1-13.
2. Donlan, R.M. and J.W. Costerton, *Biofilms: Survival mechanisms of clinically relevant microorganisms.* Clinical Microbiology Reviews, 2002. **15**(2): p. 167-193.
3. Rhoads, D.D., R. Wolcott, and S.L. Percival, *Biofilms in wounds: management strategies.* Journal of Wound Care, 2008. **17**(11): p. 502-508.
4. Kaplan, J.B., *Biofilm dispersal: Mechanisms, clinical implications, and potential therapeutic uses.* Journal of Dental Research, 2010. **89**(3): p. 205-218.
5. Akers, K.S., et al., *Biofilms and persistent wound infections in United States military trauma patients: a case–control analysis.* BMC Infectious Diseases, 2014. **14**(190): p. 1-11.
6. Davis, S. and A. Nusbaum, *What is new in debridement?*, in *Advances in Wound Care*, C. Sen, Editor. 2010, Mary Ann Liebert: New Rochelle, NY. p. 535-541.
7. Rosenberg, L., et al., *Selectivity of a bromelain based enzymatic debridement agent: a porcine study.* Burns, 2012. **38**(7): p. 1035-1040.
8. Doerler, M., et al., *Impact on wound healing and efficacy of various leg ulcer debridement techniques.* Journal of the German Society of Dermatology, 2012. **10**(9): p. 624-632.
9. Bolton, L. and A.J. Fattu, *Topical agents and wound healing.* Clinics in Dermatology, 1994. **12**(1): p. 95-120.
10. Oliveira, H.L.C.D., et al., *Influence of papain in biofilm formed by methicillin-resistant Staphylococcus epidermidis and methicillin-resistant Staphylococcus haemolyticus isolates.* Brazilian Journal of Pharmaceutical Sciences, 2014. **50**(2): p. 261-267.
11. Watters, C.M., et al., *Enzymatic degradation of in vitro Staphylococcus aureus biofilms supplemented with human plasma.* Infection and Drug Resistance, 2016. **9**: p. 71-78.
12. Food and Drug Administration, *Topical drug products containing papain; enforcement action dates*. Docket No. FDA–2008–N–0481. Federal Register, 2008. **73**(185): p. 54831-54834.
13. Liu, J., et al., *Zinc oxide nanoparticles as adjuvant to facilitate Doxorubicin intracellular accumulation and visualize pH-responsive release for overcoming drug resistance.* Molecular Pharmacology, 2016. **13**(5): p. 1723-1730.
14. Puvvada, N., et al., *Novel ZnO hollow-nanocarriers containing paclitaxel targeting folate-receptors in a malignant pH-microenvironment for effective monitoring and promoting breast tumor regression.* Scientific Reports, 2015. **5**(11760): p. 1-15.
15. Raghupathi, K.R., R.T. Koodali, and A.C. Manna, *Size-dependent bacterial growth inhibition and mechanism of antibacterial activity of zinc oxide nanoparticles.* Langmuir, 2011. **27**(7): p. 4020-4028.
16. Chen, C.W., et al., *Metal nanobullets for multidrug resistant bacteria and biofilms.* Advanced Drug Delivery Reviews, 2014. **78**: p. 88-104.
17. Dwivedi, S., et al. *Reactive oxygen species mediated bacterial biofilm inhibition via zinc oxide nanoparticles and their statistical determination*. PLoS One, 2014. **9**(11): p. e111289, DOI: 10.1371/journal.pone.0111289.
18. Azam, A., et al., *Antimicrobial activity of metal oxide nanoparticles against gram-positive and gram-negative bacteria: A comparative study.* International Journal of Nanomedicine, 2012. **7**: p. 6003-6009.

19. Khan, S.T., et al., *Anti-biofilm and antibacterial activities of zinc oxide nanoparticles against the oral opportunistic pathogens Rothia dentocariosa and Rothia mucilaginosa.* European Journal of Oral Sciences, 2014. **122**(6): p. 397-403.
20. Pati, R., et al., *Topical application of zinc oxide nanoparticles reduces bacterial skin infection in mice and exhibits antibacterial activity by inducing oxidative stress response and cell membrane disintegration in macrophages.* Nanomedicine: Nanotechnology, Biology, and Medicine, 2014. **10**(6): p. 1195-1208.
21. Ansari, M.A., et al., *Characterization of clinical strains of MSSA, MRSA and MRSA isolated from skin and soft tissue infections and the antibacterial activity of ZnO nanoparticles.* World Journal of Microbiology & Biotechnology, 2012. **28**(4): p. 1605-1613.
22. Kumar, S., et al., *Evaluation of wound healing potential of beta-chitin hydrogel/nano zinc oxide composite bandage.* Pharmaceutical Research,, 2013. **30**(2): p. 523-537.
23. Xie, Y., et al., *Antibacterial activity and mechanism of action of zinc oxide nanoparticles against Campylobacter jejuni.* Applied and Environmental Microbiology, 2011. **77**(7): p. 2325-2331.
24. Dizaj, S.M., et al., *Antimicrobial activity of the metals and metal oxide nanoparticles.* Materials Science and Engineering: C, 2014. **44**: p. 278-284.
25. McGuffie, M.J., et al., *Zinc oxide nanoparticle suspensions and layer-by-layer coatings inhibit staphylococcal growth.* Nanomedicine, 2016. **12**(1): p. 33-42.
26. Sirelkhatim, A., et al., *Review on zinc oxide nanoparticles: antibacterial activity and toxicity mechanism.* Nano-Micro Letters, 2015. **7**(3): p. 219-242.
27. Deng, C., et al., *Facile template-free sonochemical fabrication of hollow ZnO spherical structures.* Materials Letters, 2010. **64**(7): p. 852-855.
28. Pinto, C., et al., *Determination of papain activity in topical dosage forms: single laboratory validation assay.* Latin American Journal of Pharmacy, 2007. **26**(5): p. 771-775.
29. Zhao, X. and L. Qi, *Rapid microwave-assisted synthesis of hierarchical ZnO hollow spheres and their application in Cr(VI) removal.* Nanotechnology, 2012. **23**(235604): p. 1-7.
30. Yedurkar, S., C. Maurya, and P. Mahanwar, *Biosynthesis of zinc oxide nanoparticles using Ixora Coccinea leaf extract—A green approach.* Open Journal of Synthesis Theory and Applications, 2016. **5**: p. 1-14.
31. Muhammad, F., et al., *Acid degradable ZnO quantum dots as a platform for targeted delivery of an anticancer drug.* Journal of Materials Chemistry, 2011. **21**(35): p. 13406-13412.
32. Zhang, B., et al., *Papain/Zn3(PO4)2 hybrid nanoflower: preparation, characterization and its enhanced catalytic activity as an immobilized enzyme.* RSC Advances, 2016. **6**(52): p. 46702-46710.
33. Sharma, M., et al., *Enteric microsphere formulations of papain for oral delivery.* Yakugaku Zasshi-Journal of the Pharmaceutical Society of Japan, 2011. **131**(5): p. 697-709.
34. Berg, J.M., et al., *The relationship between pH and zeta potential of ~ 30 nm metal oxide nanoparticle suspensions relevant to in vitro toxicological evaluations.* Nanotoxicology, 2009. **3**(4): p. 276-283.
35. Qadeer, A., M. Zaman, and R.H. Khan, *Inhibitory effect of post-micellar SDS concentration on thermal aggregation and activity of papain.* Biochemistry (Moscow), 2014. **79**(8): p. 785-96.

REPORT DOCUMENTATION PAGE

1. REPORT DATE (DD MM YY)
September 12, 2019

2. REPORT TYPE
Technical Report

3. DATES COVERED (from – to)
May 2016 - September 2019

4. TITLE
Development of Multifunctional ZnO Nanocarriers for Controlled and Enhanced Biofilm Dispersion

5a. Contract Number:
5b. Grant Number:
5c. Program Element Number:
5d. Project Number:
5e. Task Number:
5f. Work Unit Number: G1701

6. AUTHORS
Zakiya Skeete, Sara Row, Dickson Kirui, Nancy J. Millenbaugh

7. PERFORMING ORGANIZATION NAME(S) AND ADDRESS(ES)
Naval Medical Research Unit San Antonio
3610 Chambers Pass, Bldg. 3610
Joint Base San Antonio-Ft. Sam Houston, TX 78234

8. PERFORMING ORGANIZATION REPORT NUMBER
NAMRU-SA REPORT # 2020-05

9. SPONSORING/MONITORING AGENCY NAMES(S) AND ADDRESS(ES)
In-house Laboratory Independent Research
503 Robert Grant Ave., Bldg. 500
Silver Spring, MD 20910

10. SPONSOR/MONITOR'S ACRONYM(S)
ILIR

11. SPONSOR/MONITOR'S REPORT NUMBER(s)

12. DISTRIBUTION/AVAILABILITY STATEMENT
Approved for public release; distribution is unlimited.

13. SUPPLEMENTARY NOTES
N/A

14. ABSTRACT
The goal of this study was to develop ZnO nanocarriers for the delivery of the enzymatic debridement agent papain as a potential treatment for chronic biofilm infections. A sonochemical method was used to synthesize papain-loaded ZnO nanoparticles (ZnO-Pap NPs) and resulted in spherical nanoshells with dry diameters of 177±50nm. Papain incorporation into the nanocarriers was confirmed by the presence of protein functional groups detected via Fourier transform infrared spectroscopy. Analysis of the loading efficiency of papain into the nanocarriers showed a protein content of 168±8µg/mg of NPs, of which 41% was enzymatically active. Scanning electron microscopy indicated the particles were structurally stable over 28 days of storage under wet or dry conditions. However, dynamic light scattering analysis revealed that the particles were prone to aggregation after 2 days of wet or dry storage. The ZnO-Pap NPs exhibited increased dissolution at pH 5 and 6 compared to neutral pH, indicating the possibility for pH-triggered papain delivery at acidic microenvironments within biofilms. The results obtained from this preliminary investigation demonstrate the potential of ZnO to act as a papain nanocarrier system. Further studies need to be conducted to optimize particle stability during storage, papain loading efficiency, and the kinetics of papain release.

15. SUBJECT TERMS
Papain, Zinc oxide nanocarriers, Biofilm dispersal, Sonochemical

16. SECURITY CLASSIFICATION OF:			17. LIMITATION OF ABSTRACT	18. NUMBER OF PAGES	19a. NAME OF RESPONSIBLE PERSON
a. REPORT	b. ABSTRACT	c. THIS PAGE			CAPT Andrew F. Vaughn, MC, USN
UNCL	UNCL	UNCL	UNCL	29	19b. TELEPHONE NUMBER (INCLUDING AREA CODE) COMM/DSN: 210-539-5334 (DSN: 389)